Desalination and Water Treatment
www.deswater.com

doi: 10.5004/dwt.2021.27769

239 (2021) 228–240
November

Heterogeneous activation of persulfate by iron/graphene oxide-MCM for removing levofloxacin hydrochloride in water

Xu Wang[a], Xiulei Zhang[a], Dongyan Zhang[b], Weiwei Chen[a], Ying Sun[a], Wenda Zuo[a], Ping Guo[a,c,*]

[a]*Key Laboratory of Groundwater Resources and Environment Ministry of Education, College of New Energy and Environment, Jilin University, Changchun 130012, China, emails: guoping@jlu.edu.cn (P. Guo), wangxujlu@outlook.com (X. Wang), 1564843948@qq.com (X. Zhang), 65562736@qq.com (W. Chen), 837901193@qq.com (Y. Sun), 1733762925@qq.com (W. Zuo)*
[b]*The First Hospital of Jilin University, Changchun 130021, China, email: 277374115@qq.com*
[c]*State Key Laboratory of Superhard Materials, Jilin University, Changchun, China*
[†]*These authors contributed equally to this paper.*

Received 23 May 2021; Accepted 7 September 2021

ABSTRACT

Iron/graphene oxide (GO) – MCM (FGM), a synthesized catalyst prepared via solvothermal method was characterized and applied in persulfate (PS) activation. FGM possessed abundant trivalent iron and defect sites which participated PS activation and contributed to the removal of levofloxacin hydrochloride (LH). LH removal efficiency reached 97% within 10 min in FGM/PS system via radical and non-radical pathways under mild conditions (20°C and neutral condition), and the mechanisms of removing LH, mainly $SO_4^{\bullet-}$ and $^{\bullet}OH$ generations during PS activation, depended on pH and temperature. $SO_4^{\bullet-}$ and $^{\bullet}OH$ were dominated at strong acid condition and at weak acid/alkaline condition, respectively. The generation of $^{\bullet}OH$ negatively correlated with temperature, but $SO_4^{\bullet-}$ generation as a function of temperature nonlinearly changed. Except adsorption, the other non-radical pathway such as defect sites in GO of FGM might also take part in LH removal. FGM under diverse conditions presented great stability while few release of free iron ions had no influence on the LH removal. Thus, a new synthesized catalyst with distinguished catalytic ability and excellent stability has been prepared for efficiently treating organic pollutants in water.

Keywords: Persulfate activation; Graphene oxide; Levofloxacin hydrochloride; Radical and non-radical

1. Introduction

Antibiotic pollution has become a worldwide problem due to the mobility and persistence of antibiotics in environment. Fluoroquinolones, one of the widely used antibiotics have been produced and overused extensively as the broad spectrum, strong tissue penetration and other excellent qualities of bacterial infection treatment [1]. Although fluoroquinolones could be absorbed by human bodies and livestock, massive fluoroquinolones were still detected at concentrations ranging from ng/L to mg/L in different environmental compartments because of incomplete metabolism in the target organism, inefficient wastewater treatment or inappropriate disposal of expired fluoroquinolones [2]. Concentrated fluoroquinolones in environment could induce a selective pressure on bacteria, leading to the occurrence of antibiotic resistant bacteria and antibiotic resistant genes in ecosystem [3]. Hence, it is very necessary to develop the efficient treatment techniques for removing fluoroquinolones from polluted environmental components.

Advanced oxidation processes, including Fenton method, ozone oxidation, electrochemical oxidation, photocatalysis oxidation and wet oxidation, are promising strategies for

* Corresponding author.

treating antibiotic wastewater [4,5]. Persulfate (PS) activation technique, an emerging advanced oxidation technology, has attracted massive attentions in recent years because the strong oxidizing sulfate radical ($SO_4^{\bullet-}$) generated through activation has a high oxidation potential (2.5–3.1 V) for the degradation of refractory organic pollutants in the water. It has been reported that $SO_4^{\bullet-}$ possesses a higher selectivity for oxidation and a better flexibility of pH tolerance compared with the hydroxyl radical ($^{\bullet}OH$) from Fenton or Fenton-like reaction [6–9]. Zhang et al. [10] established PS activation by biochar and 90% tetracycline, chlortetracycline and doxycycline were degraded in 40 min due to the generations of $SO_4^{\bullet-}$ and $^{\bullet}OH$. Chokejaroenrat et al. [11] demonstrated that a small continual input of zero valent iron could sufficiently activate PS and generate $SO_4^{\bullet-}$ to remove 68% sulfadimethoxine from filtered discharge water. Traditional methods for activating PS include UV-light irradiation, heat, transition metal ion and semi-conductors [12–16]. However, extra equipment and energy consumption of photo and thermal activators, homogeneous catalyst issues which are secondary pollution of toxic transition metal ions and pH-dependent activating performances limit the application of PS activation technique in wastewater treatment. Therefore, heterogeneous catalyst with high activation efficiency, few chemicals required and great stability [17,18] will be an exceptional solution.

The improvement of PS activation technique on antibiotic wastewater treatment mainly depends on developing the new heterogeneous catalyst and studying the factors influencing catalysis to date. Transition metal-based catalysts are commonly applied in PS activation industry at present [19]. Divalent iron outcompetes other transition metal because it is environmentally friendly, relatively nontoxic and cost-effective [20]. Almost all iron-catalytic systems in industrial treatment are homogeneous reactions, thus leading to several problems such as energy waste and greenhouse gases exhausting [19]. The factor that Fe(II) at high concentration could scavenger sulfate radical markedly limits the catalytic performance of PS by free Fe(II) [21]. Thus, heterogeneous catalysts bonded with iron or iron oxides should be extensively investigated [22]. The mesoporous MCM-41 molecular sieve is one of the most popular silicon carrier for heterogeneous catalyst because of its lattice defects, no acid center and great hydrothermal stability [23]. However, the simple catalyzing mechanisms have confined the catalyzing capabilities of MCM-41 doped or mixed with active metals [24,25]. Carbonaceous materials, such as carbon nanotube, graphene oxide (GO) and fullerene can activate PS by multiple pathways due to their large surface area, promising semiconductivity, strong substrate-catalyst interaction and high defect site configuration [26–29]. Therefore, compound catalyst composing of active metal, carbonaceous material and molecular sieve may significantly improve the removal efficiencies of refractory organic pollutants by activating PS because relevant catalyst possesses multiple degradation pathways, potential stability and great catalytic performance.

Hence, a novel metal–nonmetal compound catalyst, iron/graphene oxide (GO) – MCM (FGM), used for PS activation was prepared with solvothermal method in this work. Scanning electron microscope (SEM), X-ray diffraction (XRD), Raman spectra and X-ray photoelectron spectroscopy (XPS) were conducted for the characterization of catalyst. Levofloxacin hydrochloride (LH) is one of the typical fluoroquinolones for treating bacterial infection by inhibiting the activity of bacterial DNA helicase [6] and used as removal target fluoroquinolones in this paper. The efficiencies of LH removal was determined in PS activation systems where various catalysts were applied. Meanwhile, the removal mechanisms of radical and non-radical pathways were clarified by radical quenching and adsorbing experiments. Furthermore, experimental conditions influencing PS activation, including catalyst dosage, oxidant concentration, pH and temperature were studied, and the catalyst stability was assessed.

2. Experimental section

2.1. Chemicals and materials

All chemicals were of analytical grade. MCM-41 and graphene oxide (GO) were purchased from Nankai University Catalyst Plant and Aladdin Reagent (Shanghai) Co., Ltd. $FeSO_4{\cdot}7H_2O$, NaOH and $Na_2S_2O_8$were provided by Sinopharm Chemical Reagent Beijing Co., Ltd. Methanol (MeOH) and tert butyl alcohol (TBA) as radical capturer were provided by Xilong Chemical Co., Ltd. Levofloxacin hydrochloride in reagent degree was purchased from Kuer Bioengineering Co., Ltd., in Anhui, China.

2.2. Catalyst preparation

Solvothermal method conducted in sealed reactor under high temperature and high pressure was applied to prepare catalyst [30]. Briefly, $FeSO_4{\cdot}7H_2O$ and MCM-41were selected as iron source and carrier, respectively. Appropriate amount of MCM-41 was dispersed into ethanol water solution at 1:1 in volume, and GO solution (7.75 mg/mL) was added into solution. The concoction was under ultrasonic for 20 min, then stirred and refluxed at 110°C for 4 h. Mixed $FeSO_4{\cdot}7H_2O$ and hot solution, stirred for another 2 h. The change in mixed solution appearance was observed from brown black to fully dark. Suspended matter was filtered from water and washed repeatedly by ethanol. Clean dark solid was freezing dried for 15 h, triturated into black powders. The other MCM-based catalysts, that is, Fe-MCM and GO-MCM were prepared used by solvothermal method too. Fe-MCM was prepared when no GO was added following above steps and GO-MCM was prepared when no $FeSO_4{\cdot}7H_2O$ was dispersed following above steps.

2.3. Characterizations

Powder XRD patterns of catalysts were measured on Labx XRD-6000 diffractometer (Shimadzu, Japan) using Cu Ka source in the scan range of 0.5°–10° for low-angle analysis and scan range of 10°–90° for wide-angle analysis at a scan step of 0.02°. Raman spectra were measured using a Raman spectrometer (HORIBA LabRAM HR) equipped with an argon ion laser emitting at 633 nm. The morphology of catalysts was observed by Magellan-400 scanning electron microscope. Surface area and mean pore diameter of FGM were obtained by Brunauer–Emmett–Teller

(BET) method. And XPS of FGM was conducted by Phi-5000Versaprobe XPS instrument for analyzing the chemicals states, and XPS high-resolution spectra of O1s, C1s and Fe2p were obtained.

2.4. Experimental and analytical procedures

The catalysts included the tested catalyst (FGM) and the control catalysts (Fe-MCM, GO-MCM, Fe, that is, $FeSO_4$ and GO). 0.05 g catalyst and 0.02 g oxidant, the persulfate (PS, $Na_2S_2O_8$) were successively added into 250 mL conical bottle with 100 mL LH solution at 100 mg/L (diluted from concentrated solution, stored in dark, pH was not adjusted and equaled 4.3). The pre experiment demonstrated that the removal efficiencies peaked at 10 min (Fig. S1) with 0.35405 min^{-1} of the reaction rate constant in FGM/PS. Solution was stirred at 20°C for 10 min and sampled from reaction system for measuring LH concentration and other analysis. Adsorption capacity of catalyst was measured in absence of PS. Besides, radical quenching experiments were conducted to elucidate how radical pathway influenced LH removal efficiency. Briefly, appropriate volumes of the LH, alcohol (10 mol/L MeOH or 10 mol/L TBA) and PS were sequentially added to achieve the same reactant concentrations. The effects of each constituent of FGM on removing LH were discovered and the factors influencing FGM/PS system, including catalyst dosage, oxidizing agent concentration, solution pH and temperature were discussed.

The concentration of LH was determined by a high performance liquid chromatography (HPLC, CFTGC-211-048, Waters, US) at the following conditions: detection wavelength: 293 nm; mobile phase: a mixture of phosphoric acid solution (0.04 mol/L, pH = 4 adjusted by three ethylamine) and acetonitrile at the volume ratio of 85/15; flow rate: 1.0 mL/min; column temperature: 30°C. Then the LH removal efficiencies were calculated. Dissolved iron concentration was measured by spectrophotometric determination of phenanthroline. The dissolved iron rate, that is, the ratio of iron concentration in reaction system and iron content in catalyst was computed.

3. Results and discussion

3.1. Characterizations

Wide-angle (a) and low-angle (b) XRD patterns of MCM-41, Fe-MCM and FGM are shown in Fig. 1. Four well resolved peaks, 100, 110, 200 and 210 reflections of MCM-41 curve from low-angle XRD pattern confirmed the ordered mesoporous structure of MCM-41 [31]. The low-angle XRD patterns of Fe-MCM and FGM shared the exactly same peak positions as MCM-41, which demonstrated that both Fe-MCM and FGM also contained the ordered pores and the crystal cell size identical with MCM-41. The same results were obtained from Fig. 1a. All of three materials showed strong peaks at 2θ of 5.9° and 22.4°, which indicated they had similar crystal framework. Although the intensities of small angle area (4°–7°) slightly decreased because of a little loss of the ordered pores after GO and Fe were mixed with MCM-41, FGM was still highly ordered. The intensity of 100 reflection was significantly enhanced after Fe was mixed

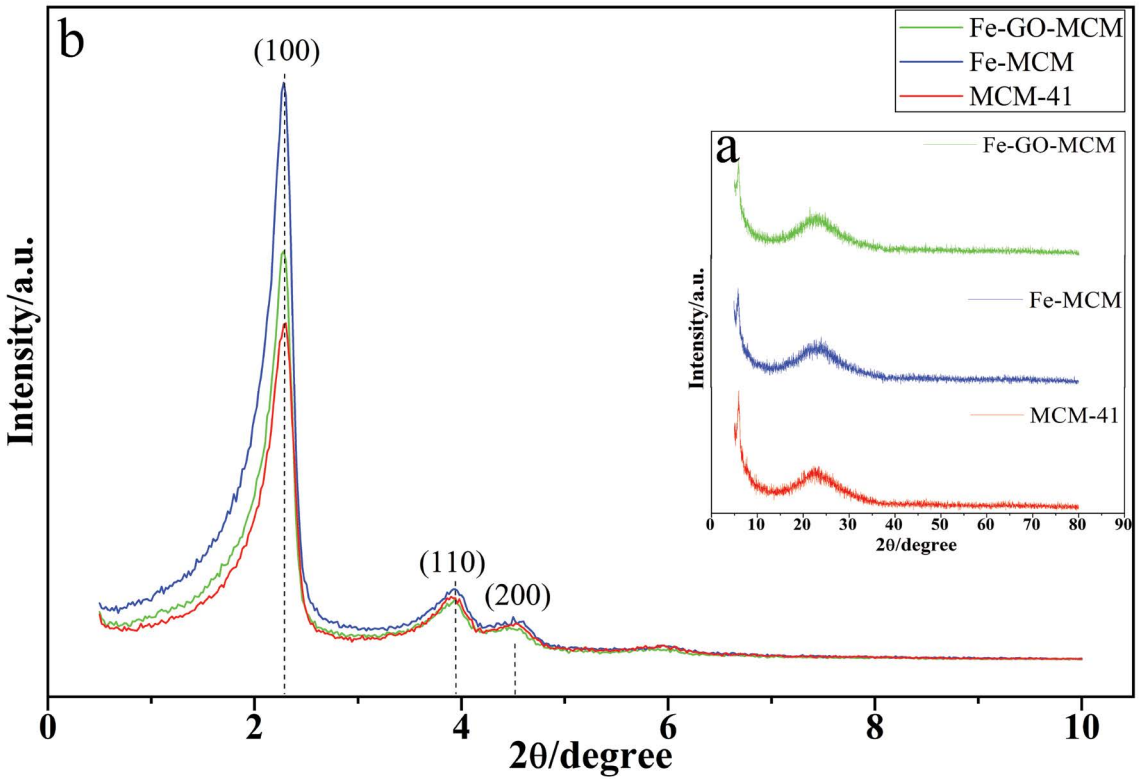

Fig. 1. Wide-angle (a) and low-angle (b) XRD patterns of MCM-41, Fe-MCM and FGM.

with MCM-41. It could be explained by preferred orientation caused by columnar growth alongside 100 reflection or more exposures of 100 reflection.

Many researches have reported that defective sites of GO can effectively activate PS to oxidize organic matters [26,27]. Raman spectroscopy is widely applied to demonstrate the defect sites of catalysts involved with carbon-based material. Raman results in Fig. 2 display that FGM and GO had similar spectral characteristic peaks' positions at 1,355; 1,595 and 2,675 cm^{-1}, which were assigned to D bond, G bond and 2D bond of carbon materials, respectively. The spectra patterns indicated that GO in FGM kept graphene-like structure. However, the intensity of every bond in GO spectra was stronger than that in FGM spectra, and he intensity ratio I_D/I_G of FGM was 0.748 and lower than that of GO (0.843). Thus less defect sites were detected in FGM than original GO.

Fig. 3 showed the SEM images of GO, MCM-41, Fe-MCM and FGM structures. The layer structure of GO is clearly observed in Fig. 3a [32], and the mesoporous structure of MCM-41 is also confirmed from Fig. 3b, which agreed with the low-angle XRD patterns. MCM-41 in the experiment was a near-spherical shape material and the diameter was around 80 μm. However, the diameter of FGM was only around 15 μm in Fig. 3d because ultrasonic wave destroyed the original MCM-41 shape and broke it into smaller pieces. Based on BET method (BET curves are shown in Fig. S2), surface area and mean pore diameter of FGM 931.86 m^2/g and 3.7545 nm. Fe-MCM surficial appearance was smoother than MCM-41 by comparing Fig. 3b and c because of even distribution of iron ion following the well-ordered mesoporous structure of MCM-41. A few GO pieces covered on the surface of MCM-41, which caused the slight loss of the ordered mesoporous structure. This phenomenon exactly interpreted the lower intensities of the small angle area in wide-angle XRD patterns.

The chemical states of FGM were investigated by XPS as shown in Fig. 4a. O1s, C1s, Fe2p and Si2p core level peaks were observed and deconvolution was conducted for XPS high-resolution spectra of O1s (Fig. 4b), C1s (Fig. 4c) and Fe2p (Fig. 4d) core level peaks. In Fig. 4b, 531, 532.7 and ~534 eV were arranged to C=O or O–C=O bonds, C–O bonds (alcohol) and physically absorbed water, respectively [33]. The peaks at 284.6, 285.6 and 286.8 eV appeared in peak division imitating analysis of C1s as the representatives of C–C bonds (sp^2-hybridized), defects C–C sp^3 and C–O bonds. The $Fe2p_{1/2}$ and $Fe2p_{3/2}$ spectra are observed at 724.4 and 711.4 eV in Fig. 4d [34]. $Fe2p_{3/2}$ spectra were further deconvoluted and the peaks at 711.6 and 709 eV were assigned to Fe(III) molecules and Fe(II) molecules. The molar ratio of Fe(III) and Fe(II) within GO-Fe-MCM exceeded 10:1, indicating that trivalent iron dominated the valence state of iron element [35]. Besides, no peak was found between 709.9 and 711.6 eV, which confirmed that iron was loaded on the MCM-41 mesoporous structure very well in the form of Fe^{3+} ions rather than in the form of Fe_2O_3 [36].

3.2. LH removal performances in FGM/PS system

LH removal performance of FGM in FGM/PS system was discussed by comparing with those in MCM-Fe+GO/PS, Fe+PS, MCM-GO/Fe+PS and GO/PS catalytic systems and demonstrated in Fig. 5. LH removal efficiencies in the FGM+PS, MCM-GO/Fe+PS, Fe+PS, MCM-Fe+GO/PS and GO/PS systems were 97.09%, 93.84%, 43.27%, 93.55% and 41.47%, respectively. LH removal efficiency of every catalytic

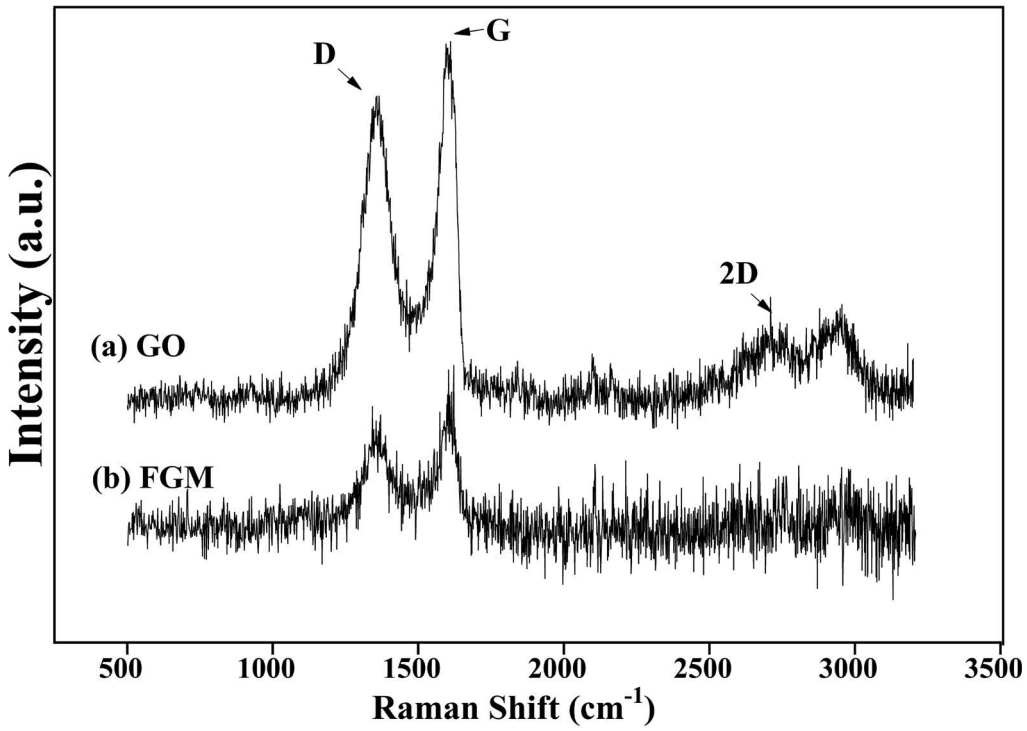

Fig. 2. Raman spectra of GO and FGM.

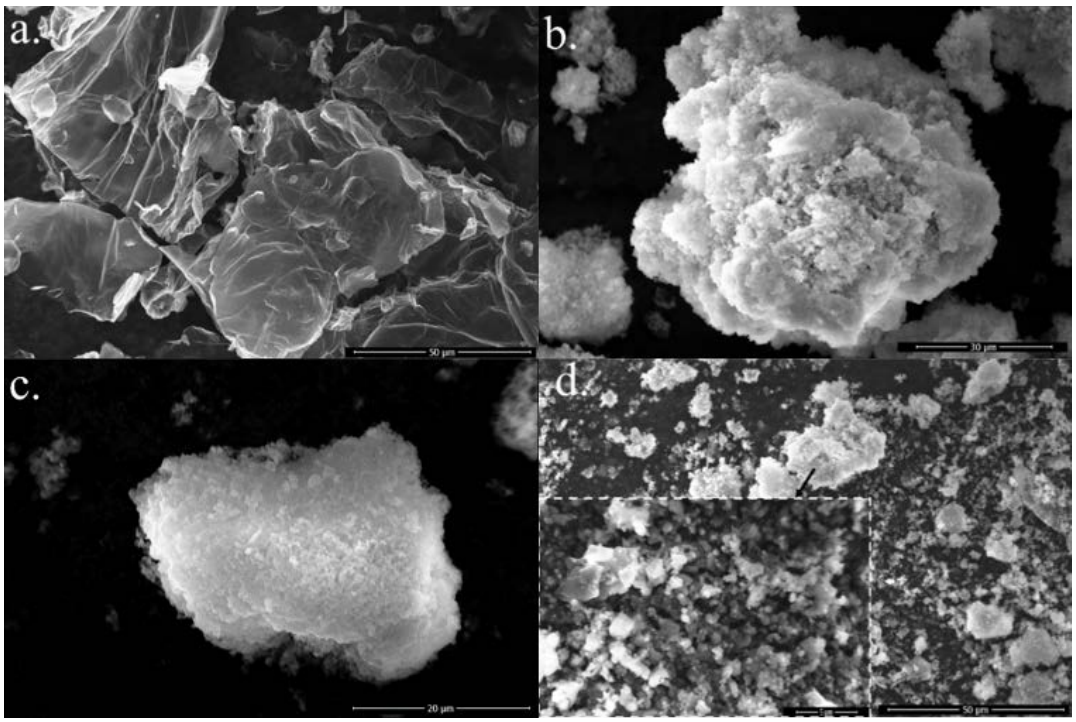

Fig. 3. SEM images of GO (a), MCM-41 (b), Fe-MCM (c) and FGM (d).

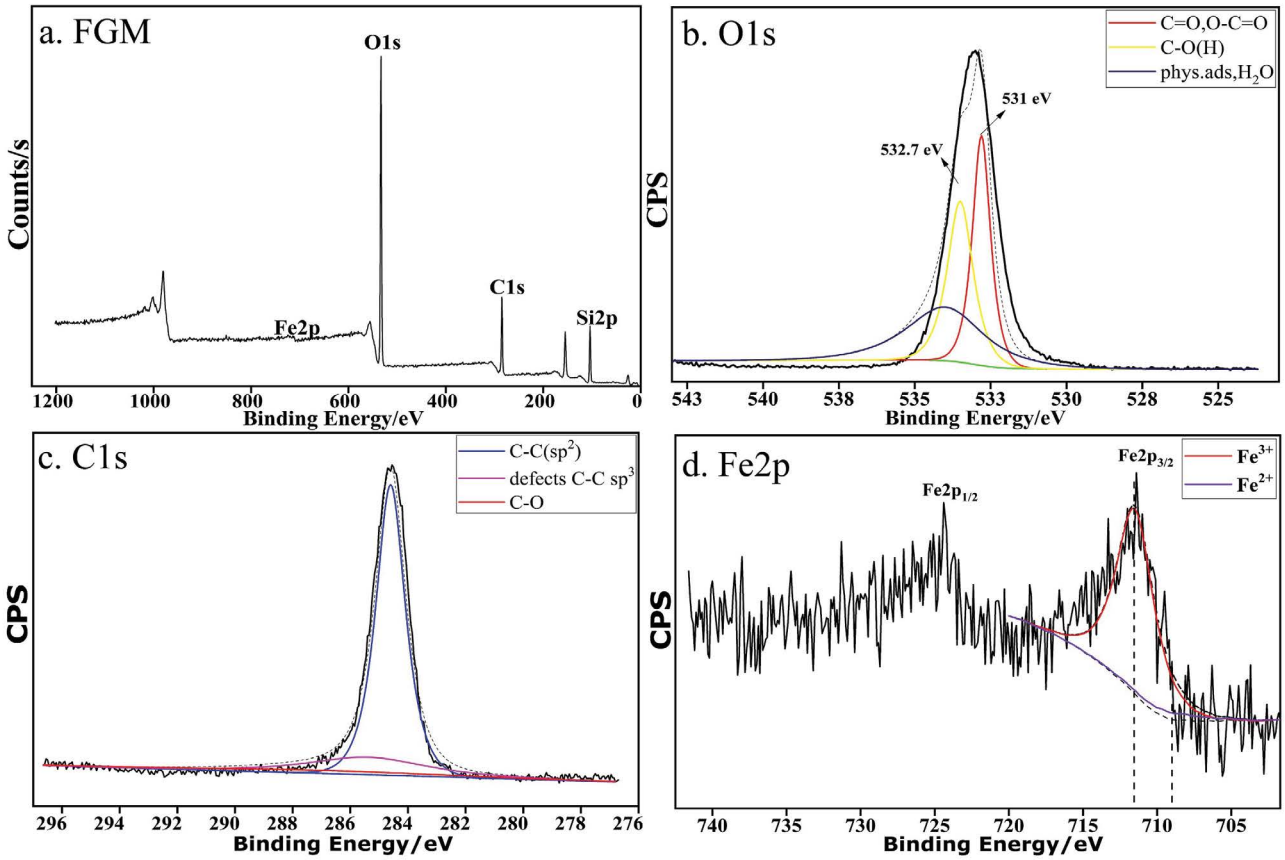

Fig. 4. XPS spectra of FGM (a), XPS high-resolution spectra of O1s (b), C1s (c) and Fe2p (d).

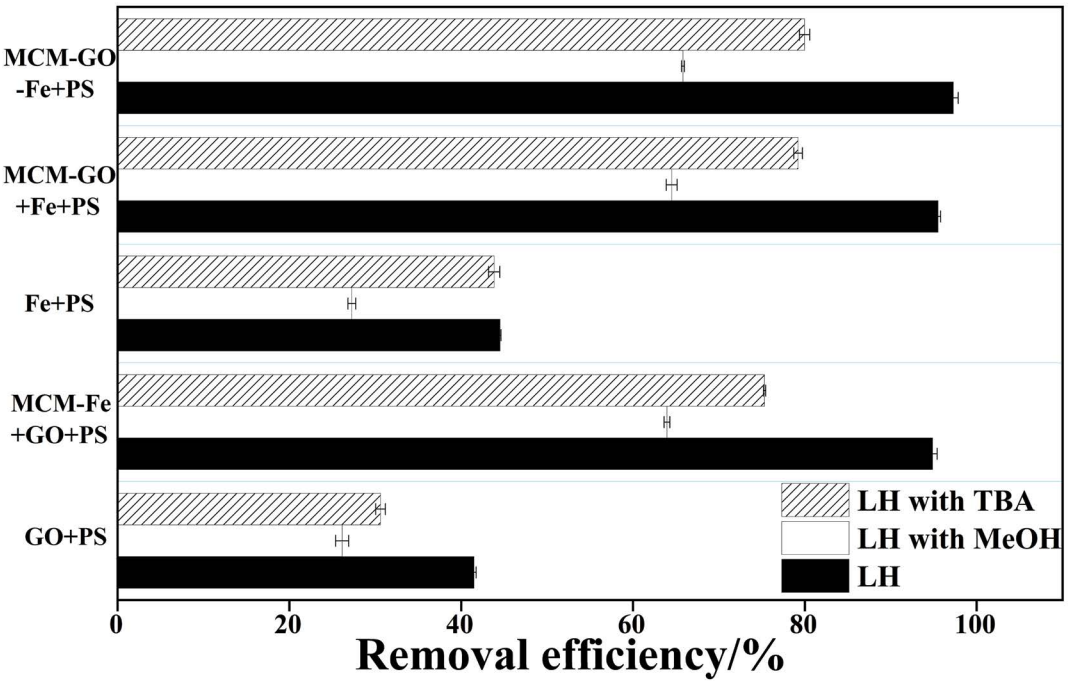

Fig. 5. The catalytic performances of FGM, GO-MCM, Fe, Fe-MCM and GO in the presence of PMS ([LH] = 100 mg/L; [catalyst] = 0.5 g/L; [PS] = 0.2 g/L; T = 20°C; pH = 4.3; t = 10 min).

system with PS was significantly higher than that without PS, whether the catalyst contained MCM. Thus, PS activation contributed to remove LH, especially the activations by MCM-base catalysts with the efficiencies up to more than 93%. Both of GO and iron in free form or bonded state in the existence of MCM could activate PS in water, and led to similar LH removal efficiencies. But the removal efficiencies in system with bonded GO or Fe was higher than those in only GO or Fe system. The differences suggested that activation of FGM on PS was more efficient than PS activations by only iron or GO.

Adsorption and radical quenching experiments were conducted to explore the differences in LH removal efficiencies of various activation systems and elucidate why FGM/PS could remove the most LH in water. Almost one-quarter of LH was removed by FGM adsorption within 10 min (shown in Fig. 6) and higher than the removal efficiencies by MCM-GO and MCM-Fe, which was attributed to small size of FGM after ultrasonic treatment, static electricity and π–π actions caused by GO [37] as well as ordered mesoporous structure of MCM. Thus, FGM possessed the biggest adsorption capability for LH, which might be an important pathway to remove organic pollutant. In addition, the adsorption capabilities of all catalysts were barely altered after adding TBA and MeOH, suggesting that radical captures did not affect adsorption capacity of catalysts and thus could be well used in radical quenching experiments.

MeOH and TBA were universally applied in radical quenching experiments as common capture agents of radicals. MeOH and TBA could quench both hydroxyl and sulfate radicals, but reaction rate of TBA and hydroxyl radical exceeded that of TBA and sulfate radical by 1000 times. Thus, the differences in LH removal efficiencies between MeOH and TBA quenching experiments in Fig. 5 demonstrate the generation of sulfate radical to some extent. LH removal efficiencies in GO/PS, Fe-MCM+GO/PS, Fe+PS, GO-MCM/Fe+PS and FGM/PS catalytic systems with MeOH or TBA at 10 min were 26.14%, 63.94%, 7.26%, 64.50% and 65.80% respectively, as well as 30.61%, 75.30%, 43.83%, 79.21% and 79.96% respectively. Removal efficiencies with MeOH were clearly lower than those with TBA. LH removal efficiencies in FGM/PS fell by around a third when MeOH were added before reacting, and by 17.32% when TBA were added. Thus, $^{\bullet}OH$ and $SO_4^{\bullet-}$ were generated and contributed to LH removal in FGM/PS. The removal efficiency in Fe+PS system with TBA was close to the efficiency without TBA, but the efficiency with MeOH was much lower than the former. Therefore, only $SO_4^{\bullet-}$ was generated from PS activation process in single iron catalytic system. However, LH removal efficiencies in GO-involved catalytic systems in presence of TBA decreased remarkably compared with the efficiencies without TBA. Additionally, the removal efficiency in GO/PS system with MeOH was slightly lower than the efficiency with TBA, which was completely different from Fe+PS system. Hence, the generations of $^{\bullet}OH$ during PS activation by FGM depended on GO mostly, and iron could create more $SO_4^{\bullet-}$. Although the valence state of iron on FGM surface was trivalence, $SO_4^{\bullet-}$ generation in FGM/PS exceeded the generation by GO/PS. Thus, some Fe(III) on FGM surface should be transformed to Fe(II). In this work, this transformation could be induced by electron transport between GO and

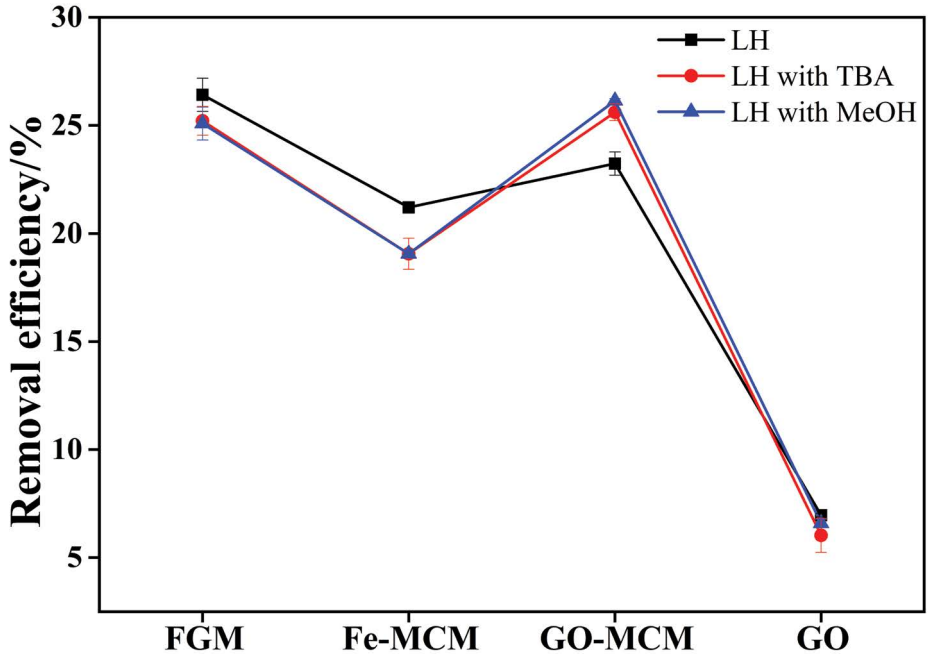

Fig. 6. Adsorption of LH by various catalysts without PS ([LH] = 100 mg/L; [catalyst] = 0.5 g/L; T = 20°C; pH = 4.3; t = 10 min).

Fe(III) on FGM surface. Firstly, Fe(III) was reduced to Fe(II) after receiving electrons from GO, then Fe(II) activated PS to generate $SO_4^{\bullet-}$ and was oxidized to Fe(III).

Except adsorption and radical pathway, other mechanisms in FGM/PS might contribute to LH removal. It has been widely reported defect sites of nano carbonaceous materials can induce a redox process between PS and organic pollutants, and they could facilitate organic degradation without any radical involved [38,39]. The sp^2-hybridized groups and sp^3 defect sites of FGM were observed from XPS spectra in section 3.1. In accordance with previous researches, Lewis basic groups like ketonic groups of nano carbons as well as zigzag edges containing unconfined π electrons, vacancies or non-six-carbon were the main defect sites in PS activation by GO [40]. Besides, the electron transport from GO to Fe(III) on FGM surface was discussed in previous paragraph, thus holes with oxidizing potential might be created in GO of FGM and oxidize LH in water.

3.3. Effect of reaction parameters on LH removals in FGM/PS system

3.3.1. Effect of FGM dosages and PS concentrations

LH removal efficiencies in FGM/PS system were impacted by FGM dosage and PS concentration as shown in Fig. 7. FGM dosage and PS concentration ranged from 0.1 to 1.0 g/L and from 0.1 to 0.5 g/L, respectively. Although LH removal efficiencies gradually increased with the catalyst dosage rising, the differences were less significant. At 0.1 g/L dosage, the LH removal efficiency was 93.05% at 10 min, and over 95% removal of LH was achieved within the catalyst dosage range from 0.3 to 1.0 g/L. Similar removal efficiencies were observed with catalyst dosages from 0.5 to 1.0 g/L, in which the LH removal efficiencies were 97%. Thus, the proper catalyst dosage for LH removal was 0.5 g/L.

LH removal efficiencies were 80.08%, 97.10%, 95.98%, 97.54% and 97.81% when the PS concentration changed from 0.1 to 0.5 g/L. LH removal efficiency with 0.2 g/L PS markedly exceeded that with 0.1 g/L PS by a huge improvement, 14.4%. LH removal efficiency with 0.5 g/L PS surpassed the efficiencies with 0.3 and 0.4 g/L by a small margin, and was equal to the efficiencies with 0.2 g/L. Following reasons might elucidate above phenomena: (1) more PS could compete with organic pollutants for free radicals and the reaction of organic pollutants with free radicals was reduced, so as to decrease the LH removal efficiency, as seen Eqs. (1) and (2); (2) the increase in PS concentration also generated more free radicals, which led to the self-cleaning phenomenon among free radicals each other, as seen equation Eq. (3). Therefore, when PS concentration was above 0.2 g/L, these negative impacts limited a further improvement of LH removal. Hence, 0.2 g/L PS was most suitable for FGM/PS system considering both removal mechanisms and economic benefit.

$$SO_4^{\bullet-} + S_2O_8^{2-} \rightarrow SO_4^{2-} + S_2O_8^{2-\bullet} \quad (1)$$

$$^{\bullet}OH + S_2O_8^{2-} \rightarrow HSO_4^- + SO_4^{\bullet-} + 1/2O_2 \quad (2)$$

$$^{\bullet}OH + SO_4^{\bullet-} \rightarrow HSO_4^- + 1/2O_2 \quad (3)$$

3.3.2. Effect of initial pH

The initial pH significantly influenced the PS activation performance of catalyst [18], thus the changes in LH removal efficiencies were determined over different initial pH values (Fig. 8). Besides, pH could alter the generation of free radicals during advanced oxidation reaction [41],

hence LH removal efficiencies were also measured in radical quenching experiments. As shown in Fig. 8, LH removal efficiencies which were above 95% kept even with the pH range from 3 to 9, and exceeded those at pH of 1 and 11. LH removal efficiency peaked at pH of 5, and reached minimum which was 80.70% at pH of 11. Thus, the optimal pH for removing LH was 5 in our work and all the LH removal efficiencies were relatively high in acid and weak base reaction condition with the pH range of 3 to 9 in this work. Hydrogen ion could deactivate •OH

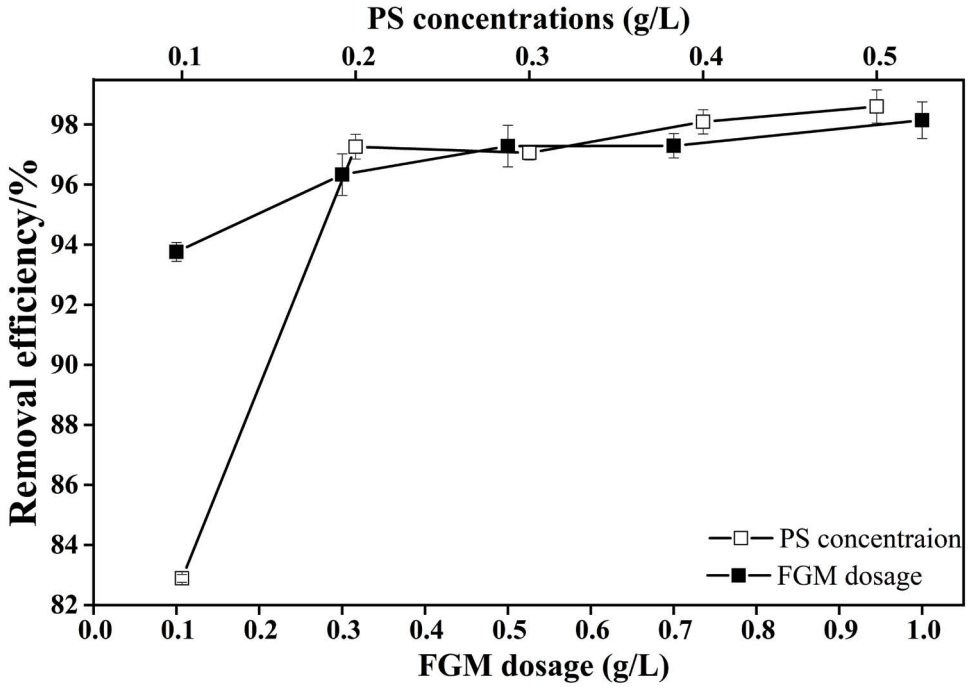

Fig. 7. LH removal efficiencies with various FGM dosage and PS concentrations in FGM/PS ([LH] = 100 mg/L; pH = 4.3; T = 20°C; t = 10 min).

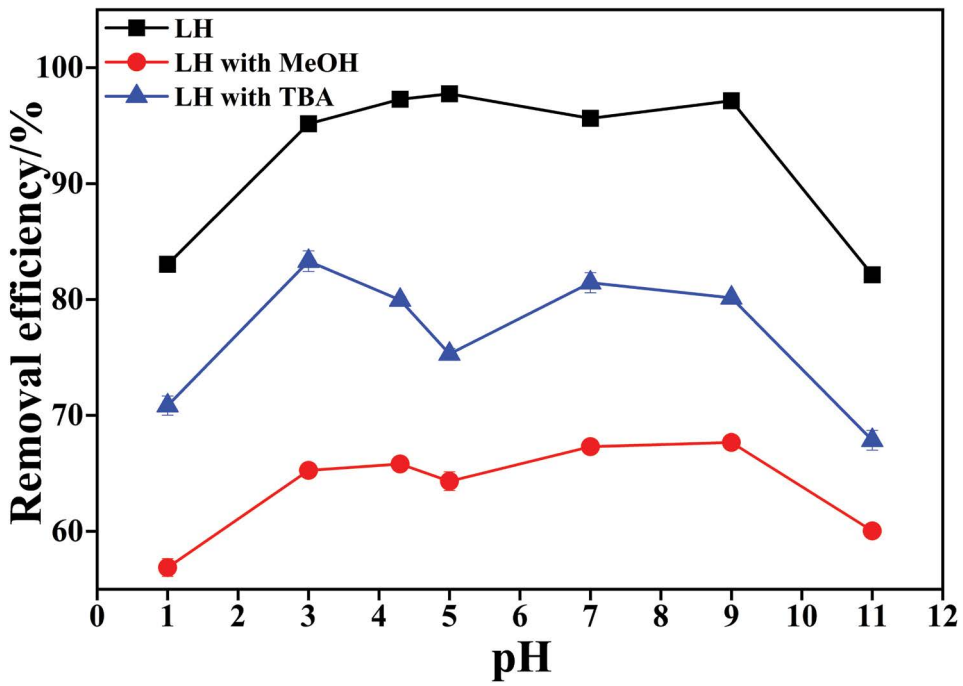

Fig. 8. LH removal efficiencies under various pH values in FGM/PS without radical capture agents and in presence of MeOH or TBA, respectively ([LH] = 100 mg/L; [FGM] = 0.5 g/L; [PS] = 0.2 g/L; T = 20°C; t = 10 min).

and $SO_4^{\bullet-}$ to some extent in PS activation process [Eqs. (4) and (5)] [18,46]. The form of LH in catalytic system might influence the reaction efficiency. Low solubility of LH in strong base solution could lead to low LH removal efficiency when pH value reached 11. Hence, high concentrations of hydrogen and hydroxyl ions reduced the organic pollutant removal efficiencies in FGM/PS system. However, LH removal efficiency under strong acid condition was even lower than that under strong base condition, which was ascribed to the self-dissociation of PS through non-radical pathway at pH of 11 [21].

$$H^+ + {}^{\bullet}OH + e^- \rightarrow H_2O \quad (4)$$

$$H^+ + SO_4^{\bullet-} + e^- \rightarrow HSO_4^- \quad (5)$$

The changes of LH removal efficiency in radical quenching experiments (in Fig. 8) reflected that $^{\bullet}OH$ and $SO_4^{\bullet-}$ generations were impacted by pH. Within pH ranging from 1 to 11, LH removal efficiencies in FGM/PS with MeOH were from 55.75% to 66.36%; and they were 69.72%, 82.91%, 78.41%, 74.18%, 80.52%, 79.21% and 66.74%, respectively in FGM/PS with TBA. Thus, the altered trends of LH removal efficiencies in MeOH and TBA quenching systems over pH values were basically similar with the alterations in total LH removal efficiencies. Both of $^{\bullet}OH$ and $SO_4^{\bullet-}$ played roles in oxidizing pollutants, but $SO_4^{\bullet-}$ was dominant at pH of 1 and 3. PS reacted with $H^{\bullet}$ of H_2O in strong acid condition (pH beneath 3) to produce some low-active substances, such as HSO_4^- (Eq. (6)), thereby reducing the LH removal through free radical pathway. More low-active substances would be created with increasing H^+ contents. Therefore, the phenomenon that the LH removal efficiency was the lowest at pH of 1 could be elucidated by the generation of low-active substances as well as Eqs. (4) and (5). At pH of 7, both $^{\bullet}OH$ and $SO_4^{\bullet-}$ participated the LH removal equally. The situations of radical generation at pH beyond 7 differed from other pH conditions. Because transformation of $SO_4^{\bullet-}$ to $^{\bullet}OH$ was enhanced [Eq. (7)] with the pH increasing [18,45], accordingly $^{\bullet}OH$ gradually became the dominant free radical at high pH values.

$$S_2O_8^{2-} + H^{\bullet} \rightarrow SO_4^{\bullet-} + HSO_4^- \quad (6)$$

$$SO_4^{\bullet-} + OH^- \rightarrow SO_4^{\bullet2-} + {}^{\bullet}OH \quad (7)$$

3.3.3. Effect of temperature

Temperature was another crucial factor for advanced oxidation reaction, hence LH removal efficiencies in FGM/PS over temperatures were measured in the existence of two radical captures (Fig. 9). Elevated temperature promoted LH removal in FGM/PS. Over 97% of LH were removed from solution under 20°C–50°C where the efficiency peaked at 50°C. Although the temperature promoted the LH removal efficiency, the increasing scope was narrow within 20°C–50°C. In other words, the improvement of LH removal by high temperatures was hardly significant after 20°C. Therefore, FGM could be efficiently applied and no extra thermal energy was needed for LH removal under normal room temperatures (25°C).

The radical generations in FGM/PS depended upon temperature variations basing on the results of radical scavenger experiments in Fig. 9. At 10°C, LH removal efficiencies were 56.87% and 69.90% in the reaction systems with MeOH

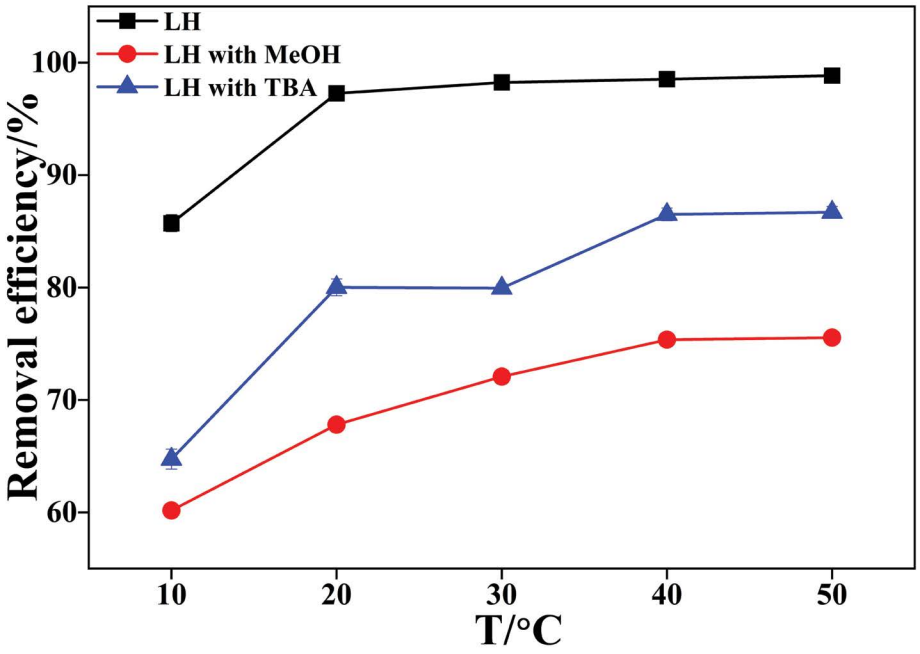

Fig. 9. LH removal efficiencies under various temperatures in FGM/PS without radical capture agents and in presence of MeOH or TBA, respectively ([LH] = 100 mg/L; [FGM] = 0.5 g/L; [PS] = 0.2 g/L; pH = 4.3; t = 10 min).

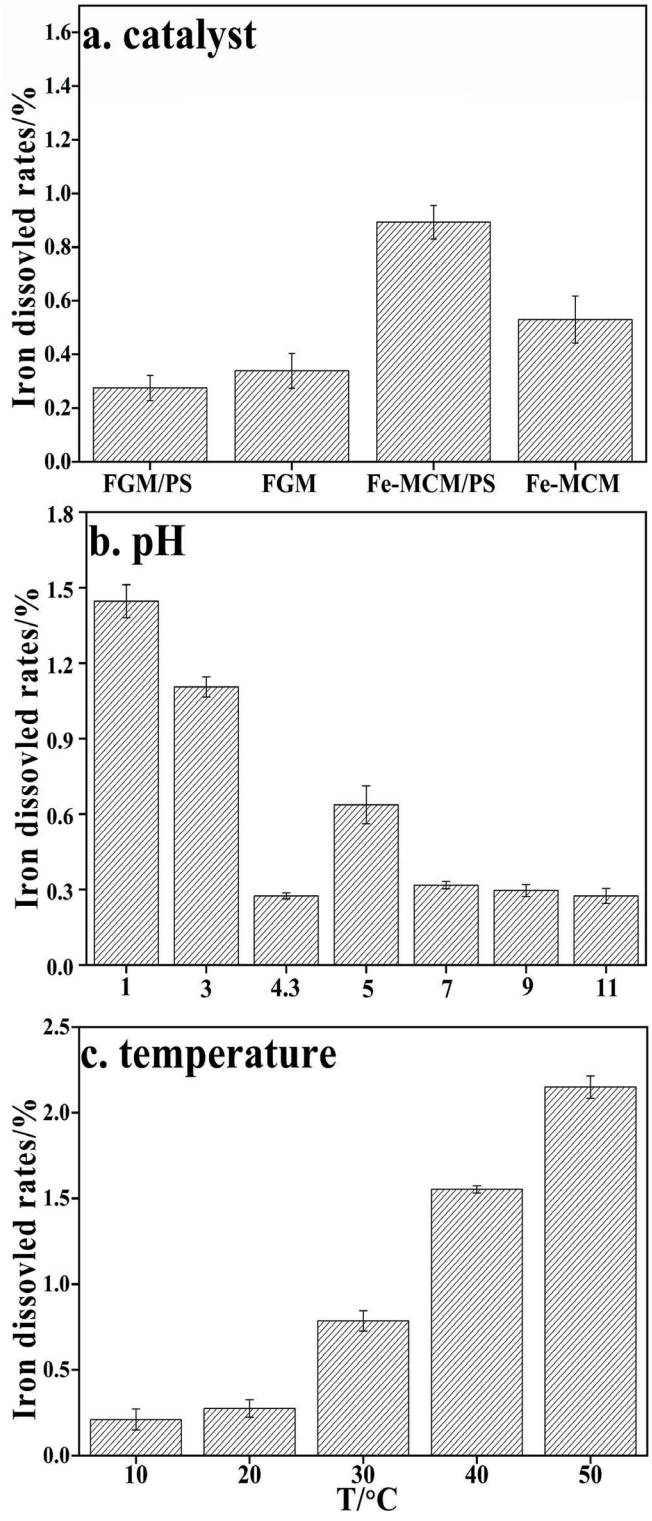

Fig. 10. The iron dissolved rates of (a) FGM and Fe-MCM with and without PS activation, (b) FGM/PS with various pH values and (c) FGM/PS with various temperatures ([LH] = 100 mg/L; [catalyst] = 0.5 g/L; [PS] = 0.2 g/L; t = 10 min).

and TBA, respectively, and at 20°C, they were 62.27% and 78.41%. LH removal efficiencies in system with MeOH remained stable, but those with TBA negatively correlated with temperature after 30°C. Therefore, the alteration of LH removal efficiencies over temperatures in the existence of radical quenchers implied obvious influence of temperatures on radical generation in FGM/PS. However, temperatures impacted sulfate and hydroxyl radical generations following different patterns. The generations of $SO_4^{\bullet-}$ above 10°C exceeded that under 10°C because $S_2O_8^{2-}$ could be activated by heat to $SO_4^{\bullet-}$ [42]. But less $SO_4^{\bullet-}$ in FGM/PS above 10°C were detected, because thermal-dependent PS activation by nano carbonaceous materials generated hydroxyl radical rather than sulfate radical over temperature [43]. Less radical generations along with higher LH removals when temperature increased from 10°C to 30°C indicated that enhanced non-radical pathways participated in removing LH. For instance, the electron transport could be improved by heat [44]. In addition, other reactive species, such as $^1O_2$, $O_2^{\bullet-}$ and H_2O_2, and direct oxidation of PS could also cause incomplete quenching [45,46]. Thus, more oxidizing holes in GO of FGM might be created and LH removal efficiency was increased. Therefore, the temperature did not only influence radical generation but impacted the non-radical pathways in removing LH.

3.4. Stability of catalyst

The stability of catalyst was assessed by calculating iron dissolved rate. The iron dissolved rates in FGM and Fe-MCM systems with and without PS were determined and the results are illustrated in Fig. 10a. All iron dissolved rates were below one percent. The lowest iron dissolved rate of 0.04% was observed in FGM/PS catalytic system and the rest rates were 0.06%, 0.10% and 0.14% for Fe-MCM/PS, FGM and Fe-MCM. The iron dissolved rates of catalysts with GO were lower compared with those of catalysts with no GO, indicating that catalyst stability was strengthened by bonded GO whether the catalytic system was in absence of PS or not. Therefore, FGM possessed an excellent stability when activating PS and removing organic pollutants. Trace free iron ions were released into catalytic system due to the outstanding stability of FGM, thus the phenomenon of radical capture by high concentration of free iron could be avoided. This might be a possible reason for great catalytic performance of FGM under various conditions.

Furthermore, the effect of pH on iron dissolved rate is shown in Fig. 10b. The dissolution rate of iron ion equaled 0.04% at pH of 4.3, and relatively higher rates (0.81%, 0.45% and 0.15%) were obtained in other acid conditions with pH of 1, 3 and 5. But dissolved iron concentrations decreased with pH increasing after pH of 5, indicating pH influenced the stability of catalyst in FGM/PS to some extent. The dissolution ascended in strong acid and alkaline solution because the solubility of mineral was sensitive to pH [44,47]. Pham et al. [39] demonstrated that the mesoporous silica under pH range from 7 to 10 conditions made the carrier unstable, and dissolved silica deposited on catalyst surface changed catalytic active sites of catalyst, thus might destroy the catalytic function of catalyst. It was deduced that pH in reaction system perhaps changed the surface characterization and mesoporous structure of FGM and influenced the bond between iron and MCM. Although

the iron dissolved rates were different within the range of pH from 3 to 9, LH removal efficiencies were barely impacted.

In addition, the effect of temperature on iron dissolved rate was investigated and shown in Fig. 10c. The iron dissolved rate increased significantly over temperatures. They were 0.04% and 0.05% at 10°C and 20°C, indicating that these two temperatures barely affected the iron dissolved rates. However, the iron dissolved rates surpassed 1% at 50°C. Therefore, the FGM stability was sensitive to temperature and high temperature was able to destroy the combination between iron and MCM/GO, especially when the temperatures were higher than normal room temperature (25°C). However, LH removal efficiency was barely influenced when the temperature changed from 20°C to 50°C. That implied that 20°C should be selected as the optimal reaction temperature, because the high temperature increased reaction cost and was adverse to catalyst stability. Different iron dissolved rates under temperatures from 20°C to 50°C along with similarly high LH removal efficiencies proved that the bonded or free iron ions barely impacted LH removal in FGM/PS.

4. Conclusion

FGM with great stability under various pH and temperatures was prepared via solvothermal method, and could effectively remove LH as a PS activator. LH removal efficiency reached 97.28% within 10 min in FGM/PS under mild conditions, which exceeded the efficiencies in Fe/PS and GO/PS by around 50% because of multiple pathways including $^{\bullet}OH$ and $SO_4^{\bullet-}$, adsorption and other potential non-radical pathways. Within the experimental range of PS and catalyst contents, relative low contents of catalyst and PS could lead to very high removal efficiencies. Temperature and pH significantly impacted the mechanisms of LH removal. LH removal efficiencies within pH range from 3 to 9 and temperature over 20°C were close and above 95%, but the mechanism except adsorption varied dramatically under same conditions. The dominant radical types in FGM/PS varied within the experimental pH range, $SO_4^{\bullet-}$ and $^{\bullet}OH$ dominated under strong acid and weak acid/alkaline conditions, respectively. In summary, this work has presented a new catalyst with excellent catalytic performance and great stability for heterogeneous PS activation, and provides an efficient removal treatment for refractory antibiotics.

Acknowledgement

This work received financial support from Open Project of State Key Laboratory of Superhard Materials (Jilin University) (No. 201809).

References

[1] H. Stephan, P.F. Matthew, R.C. Siri, P.D. Stephen, W. Paul, C. Miguel, Quinolones: from antibiotics to autoinducers, FEMS Microbiol. Rev., 35 (2011) 247–274.
[2] C. Agnieszka, P. Rama, B.S. Kaur, D. Patrick, V. Mausam, Y.S. Rao, Fluoroquinolones metal complexation and its environmental impacts, Coord. Chem. Rev., 376 (2018) 46–61.
[3] L.H. Santos, A.N. Araújo, A. Fachini, A. Pena, C. Delerue-Matos, M.C.B.S.M. Montenegro, Ecotoxicological aspects related to the presence of pharmaceuticals in the aquatic environment, J. Hazard. Mater., 175 (2010) 45–95.
[4] A. Anglada, A. Urtiaga, I. Ortiz, Pilot scale performance of the electro-oxidation of landfill leachate at boron-doped diamond anodes, Environ. Sci. Technol., 43 (2009) 2035–2040.
[5] Y.H. Chuang, A. Szczuka, F. Shabani, J. Munoz, R. Aflaki, S.D. Hammond, W.A. Mitch, Pilot-scale comparison of microfiltration/reverse osmosis and ozone/biological activated carbon with UV/hydrogen peroxide or UV/free chlorine AOP treatment for controlling disinfection byproducts during wastewater reuse, Water Res., 152 (2019) 215–225.
[6] M.A. Sarayba, N. Shamie, B.J. Reiser, P.M. Sweet, M. Taban, J.M. Graff, A. Kesler-Diaz, K.E. Osann, P.J. McDonnell, Fluoroquinolone therapy in Mycobacterium chelonae keratitis after lamellar keratectomy, J. Cataract. Refract. Surg., 31 (2005) 1396–1402.
[7] S.B. Hammouda, F. Zhao, Z. Safaei, V. Srivastav, D.L. Ramasamy, S. Iftekhar, S. Kalliola, M. Sillanpää, Degradation and mineralization of phenol in aqueous medium by heterogeneous monopersulfate activation on nanostructured cobalt based-perovskite catalysts $ACoO_3$ (A = La, Ba, Sr and Ce): characterization, kinetics and mechanism study, Appl. Catal., B, 215 (2017) 60–73.
[8] G.P. Anipsitakis, D.D. Dionysiou, Degradation of organic contaminants in water with sulfate radicals generated by the conjunction of peroxymonosulfate with cobalt, Environ. Sci. Technol., 37 (2003) 4790–4797.
[9] Y.Q. Liu, X.X. He, Y.S. Fu, D.D. Dionysou, Kinetics and mechanism investigation on the destruction of oxytetracycline by UV-254 nm activation of persulfate, J. Hazard. Mater., 305 (2016) 229–239.
[10] Y. Zhang, M. Xu, S. Liang, Z. Feng, J. Zhao, Mechanism of persulfate activation by biochar for the catalytic degradation of antibiotics: synergistic effects of environmentally persistent free radicals and the defective structure of biochar, Sci. Total Environ., 794 (2021) 148707, doi: 10.1016/j.scitotenv.2021.148707.
[11] C. Chokejaroenrat, C. Sakulthaew, A. Angkaew, T. Satapanajaru, A. Poapolathep, T. Chirasatienpon, Remediating sulfadimethoxine-contaminated aquaculture wastewater using ZVI-activated persulfate in a flow-through system, Aquacult. Eng., 84 (2019) 99–105.
[12] M.H. Nie, Y. Yang, Z.J. Zhang, C.X. Yan, X.N. Wang, H.J. Li, W.B. Dong, Degradation of chloramphenicol by thermally activated persulfate in aqueous solution, Chem. Eng. J., 246 (2014) 373–382.
[13] I. Epold, M. Trapido, N. Dulova, Degradation of levofloxacin in aqueous solutions by Fenton, ferrous ion-activated persulfate and combined Fenton/persulfate systems, Chem. Eng. J., 279 (2015) 452–462.
[14] I. Hussain, Y. Zhang, S. Huang, Q.Y. Gao, Degradation of p-chloroaniline by $FeO_{3-x}H_{3-2x}/Fe^0$ in the presence of persulfate in aqueous solution, RSC Adv., 5 (2015) 41079–41087.
[15] J. Peng, Z. Wang, S. Wang, J. Liu, Y. Zhang, B. Wang, Z. Gong, M. Wang, H. Dong, J. Shi, H. Liu, G. Yan, G. Liu, S. Gao, Z. Cao, Enhanced removal of methylparaben mediated by cobalt/carbon nanotubes (Co/CNTs) activated peroxymonosulfate in chloride-containing water: reaction kinetics, mechanisms and pathways, Chem. Eng. J., 409 (2021) 128176, doi: 10.1016/j.cej.2020.128176.
[16] M. Zou, Y. Qi, R. Qu, G. Al-Basher, X. Pan, Z. Wang, Z. Huo, F. Zhu, Effective degradation of 2,4-dihydroxybenzophenone by zero–valent iron powder (Fe^0)-activated persulfate in aqueous solution: kinetic study, product identification and theoretical calculations, Sci. Total Environ., 771 (2021) 144743, doi: 10.1016/j.scitotenv.2020.144743.
[17] I. Hussain, Y. Zhang, S. Huang, Degradation of aniline with zero-valent iron as an activator of persulfate in aqueous solution, RSC Adv., 4 (2014) 3502–3511.
[18] J.L. Wang, S.Z. Wang, Activation of persulfate (PS) and peroxymonosulfate (PS) and application for the degradation of emerging contaminants, Chem. Eng. J., 334 (2018) 1502–1517.
[19] Q. Zhao, Q. Mao, Y. Zhou, J.H. Wei, X.C. Liu, J.Y. Yang, L. Luo, J. Zhang, H. Chen, H. Chen, L. Tang, Metal-free carbon

materials-catalyzed sulfate radical-based advanced oxidation processes: a review on heterogeneous catalysts and applications, Chemosphere, 189 (2017) 224–238.
[20] W.A. Carvalho, M. Wallau, U. Schuchardt, Iron and copper immobilised on mesoporous MCM-41 molecular sieves as catalysts for the oxidation of cyclohexane, J. Mol. Catal. A: Chem., 144 (1999) 91–99.
[21] A. Rastogi, S.R. Al-Abed, D.D. Dionysiou, Sulfate radical-based ferrous-peroxymonosulfate oxidative system for PCBs degradation in aqueous and sediment systems, Appl. Catal., B, 85 (2009) 171–179.
[22] B. Zhao, X.Y. Wang, Advances in modification of mesoporous molecular sieve MCM-41 for oxidation reaction, Ind. Catal., 21 (2013) 1–5.
[23] S. Singha, K.M. Parida, A.C. Dash, Fe(III)-salim anchored MCM-41: synthesis, characterization and catalytic activity towards liquid phase cyclohexane oxidation, J. Porous Mater., 18 (2011) 707–714.
[24] M. Xia, M.C. Long, Y.D. Yang, C. Chen, W.M. Cai, B.X. Zhou, A highly active bimetallic oxides catalyst supported on Al-containing MCM-41 for Fenton oxidation of phenol solution, Appl. Catal., B, 110 (2011) 118–125.
[25] L. Bekris, Z. Frontistis, G. Trakakis, L. Sygellou, C. Galiotis, D. Mantzavinos, Graphene: a new activator of sodium persulfate for the advanced oxidation of parabens in water, Water Res., 126 (2017) 111–121.
[26] S. Karthikeyan, R. Boopathy, G. Sekaran, In situ generation of hydroxyl radical by cobalt oxide supported porous carbon enhance removal of refractory organics in tannery dyeing wastewater, J. Colloid Interface Sci., 448 (2015) 163–174.
[27] T. Kuila, S. Bose, A.K. Mishra, P. Khanra, N.H. Kim, J.H. Lee, Chemical functionalization of graphene and its applications, Prog. Mater Sci., 57 (2012) 1061–1105.
[28] H. Sun, S. Liu, G. Zhou, H.M. Ang, M.O. Tadé, S. Wang, Reduced grapheme oxide for catalytic oxidation of aqueous organic pollutants, ACS Appl. Mater. Interfaces, 4 (2012) 5466–5471.
[29] P. Zhang, J.S. Wei, X.B. Chen, H.M. Xiong, Heteroatom-doped carbon dots based catalysts for oxygen reduction reactions, J. Colloid Interface Sci., 537 (2019) 716–724.
[30] R. Ediati, P.B.F. Laharto, R. Safitri, H. Mahfudhah, D.O. Sulistiono, T.D. Syukrie, M. Nadjib, Synthesis of HKUST-1 with addition of Al-MCM-41 as adsorbent for removal of methylene blue from aqueous solution, Mater. Today:. Proc., 46 (2021) 1799–1806.
[31] W.X. Niu, R. Luque, G.B. Xu, Solvothermal synthesis of metal nanocrystals and their applications, Nano Today, 10 (2015) 240–267.
[32] Y. Nie, N. Li, C. Hu, Enhanced inhibition of bromate formation in catalytic ozonation of organic pollutants over Fe-Al LDH/Al_2O_3, Sep. Purif. Technol., 151 (2015) 256–261.
[33] X. Duan, Z. Ao, L. Zhou, H.Q. Sun, G.X. Wang, S.B. Wang, Occurrence of radical and nonradical pathways from carbocatalysts for aqueous and nonaqueous catalytic oxidation, Appl. Catal., B, 188 (2016) 98–105.
[34] G. Trakakis, G. Anagnostopoulos, L. Sygellou, A. Bakolas, J. Parthenios, D. Tasis, C. Galiotis, K. Papagelis, Epoxidized multi-walled carbon nanotube buckypapers: a scaffold for polymer nanocomposites with enhanced mechanical properties, Chem. Eng. J., 281 (2015) 793–803.
[35] X. Li, W. Chen, Y. Tang, L.S. Li, Relationship between the structure of Fe-MCM-48 and its activity in catalytic ozonation for diclofenac mineralization, Chemosphere, 206 (2018) 615–621.
[36] W. Chen, X. Li, Z. Pan, S.S. Ma, L.S. Li, Effective mineralization of Diclofenac by catalytic ozonation using Fe-MCM-41 catalyst, Chem. Eng. J., 304 (2016) 594–601.
[37] H. Sun, S. Liu, S. Liu, S.B. Wang, A comparative study of reduced graphene oxide modified TiO_2, ZnO and Ta_2O_5, in visible light photocatalytic/photochemical oxidation of methylene blue, Appl. Catal., B, 146 (2014) 162–168.
[38] C.P. Guthrie, E.J. Reardon, Metastability of MCM-41 and Al-MCM-41, J. Phys. Chem. A, 112 (2008) 3386–3390.
[39] A.L.T. Pham, D.L. Sedlak, F.M. Doyle, Dissolution of mesoporous silica supports in aqueous solutions: implications for mesoporous silica-based water treatment processes, Appl. Catal., B, 126 (2012) 258–264.
[40] C.H. Yao, Y.Q. Zhang, M.M. Du, X.D. Du, S.B. Huang, Insights into the mechanism of non-radical activation of persulfate via activated carbon for the degradation of p-chloroaniline, Chem. Eng. J., 362 (2019) 262–268.
[41] Y.H. Guan, J. Ma, Y.M. Ren, Y.L. Liu, J.Y. Xiao, L.Q. Lin, C. Zhang, Efficient degradation of atrazine by magnetic porous copper ferrite catalyzed peroxymonosulfate oxidation via the formation of hydroxyl and sulfate radicals, Water Res., 47 (2013) 5431–5438.
[42] W. Wilmarth, A. Haim, Peroxide reactions mechanisms, Inorg. Chem., 175 (1962) 976–977.
[43] X.G. Duan, S. Indrawirawan, J. Kang, W.J. Tian, H.Y. Zhang, H.Q. Sun, S.B. Wang, Temperature-dependent evolution of hydroxyl radicals from peroxymonosulfate activation over nitrogen-modified carbon nanotubes, Sustainable Mater. Technol., 18 (2018) e00082, doi: 10.1016/j.susmat.2018.e00082.
[44] L. Zhao, H. Hou, A. Fujii, M. Hosomi, F. Li, Degradation of 1,4-dioxane in water with heat- and Fe(2+)-activated persulfate oxidation, Environ. Sci. Pollut. Res., 21 (2014) 7457–7465.
[45] X. Pan, J. Chen, N. Wu, Y. Qi, X. Xu, J. Ge, X. Wang, C. Li, R. Qu, V.K. Sharma, Z. Wang, Degradation of aqueous 2,4,4′-trihydroxybenzophenone by persulfate activated with nitrogen doped carbonaceous materials and the formation of dimer products, Water Res., 143 (2018) 176–187.
[46] N.B. Oncu, N. Mercan, I.A. Balcioglu, The impact of ferrous iron/heat-activated persulfate treatment on waste sewage sludge constituents and sorbed antimicrobial micropollutants, Chem. Eng. J., 259 (2015) 972–980.
[47] H. Klöppel, A. Fliedner, W. Kördel, Behaviour and ecotoxicology of aluminium in soil and water — review of the scientific literature, Chemosphere, 35 (1997) 353–363.

Supplementary information

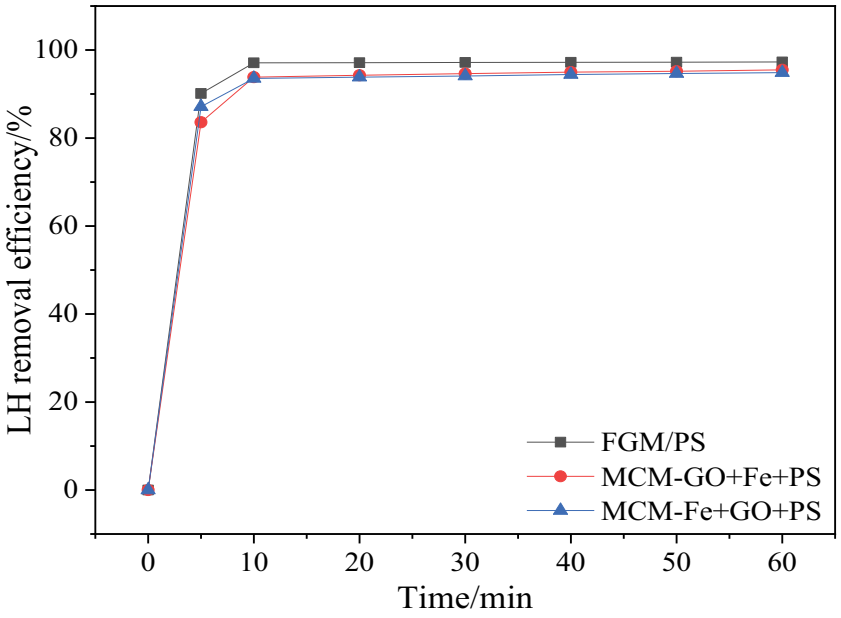

Fig. S1. Changes in LH removal efficiencies over time.

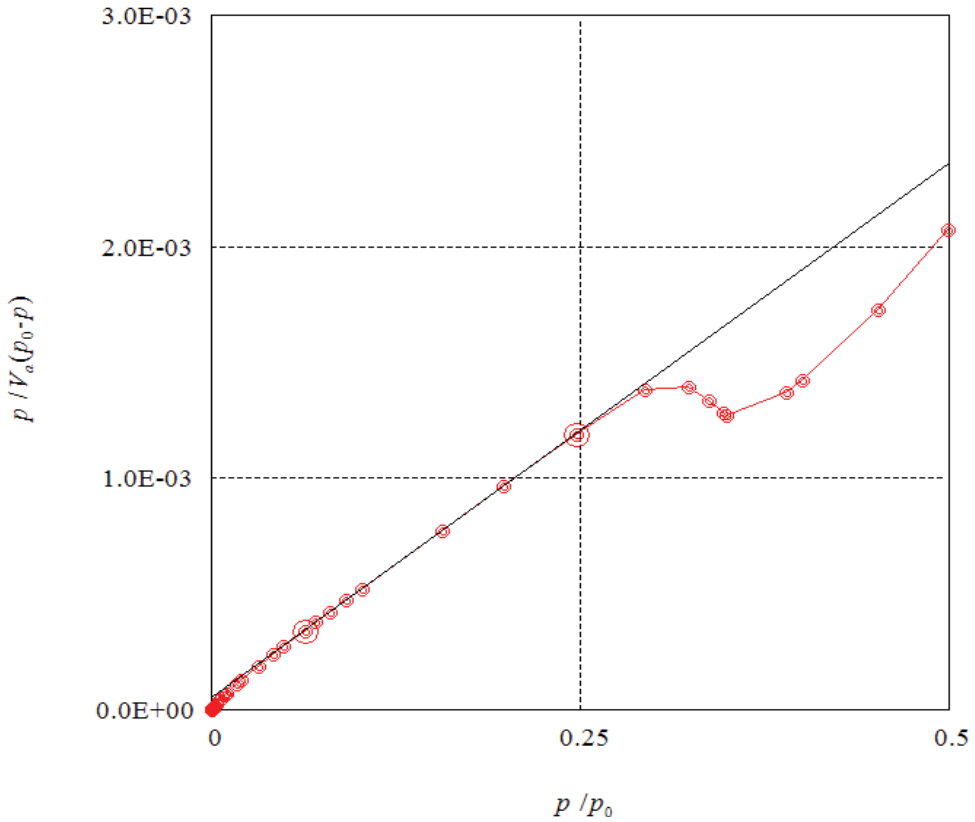

Fig. S2. BET curves of FGM.